INTERNATIONAL JOURNAL FOR NUMERICAL AND ANALYTICAL METHODS IN GEOMECHANICS
Int. J. Numer. Anal. Meth. Geomech., 2004; **28**:373–393 (DOI: 10.1002/nag.341)

Softening, localization and stabilization: capture of discontinuous solutions in J2 plasticity

M. Cervera*,†, M. Chiumenti and C. Agelet de Saracibar

International Center for Numerical Methods in Engineering (CIMNE), Technical University of Catalonia (UPC), Edificio C1, Campus Norte, Jordi Girona 1-3, Barcelona 08034, Spain

SUMMARY

This paper exploits the concept of stabilization techniques to improve the behaviour of mixed linear/linear simplicial elements (triangles and tetrahedra) in incompressible or nearly incompressible situations. Elasto-J2-plastic constitutive behaviour has been considered with linear and exponential softening. Two different stabilization methods are used to attain global stability of the corresponding discrete finite element formulation. Implementation and computational aspects are also discussed, showing that a robust application of the proposed formulation is feasible. Numerical examples show that the formulation derived is free of volumetric locking and spurious oscillations of the pressure. The results obtained do not suffer from spurious mesh-size or mesh-bias dependence, comparing very favourably with those obtained with the standard, non-stabilized, approaches. Copyright © 2004 John Wiley & Sons, Ltd.

KEY WORDS: incompressibility; plasticity; softening; localization and stabilization

1. INTRODUCTION

Softening materials subjected to monotonic straining exhibit *strain localization*. The nature of this localization depends on the particular behaviour of the material. In the so-called J2 materials, shear (or slip) strains concentrate; in Rankine-type materials, only normal elongations localize. This phenomenon leads to the formation of *localization bands* inside the solid where, once the peak stress is reached, the deformation concentrates while the material outside the band unloads elastically. This induces the formation of *weak discontinuities*, with continuous fields of displacements but discontinuous fields of strain inside and outside the bands (see Figure 1(a)).

Upon continuing straining, the width of the localization band diminishes and, unless there is a physical limitation, it tends to zero. Ultimately, this process may lead to *strong discontinuities*, with discontinuous fields of displacements across the *discontinuity line*, and unbounded strains (see Figure 1(b)). In J2 materials, these are called *slip lines*. It is generally accepted that the amount of energy released during the formation of a unit length of discontinuity line is a material property, called the *fracture energy*.

*Correspondence to: M. Cervera, ETS Ingenieros de Caminos, Canales y Puertos, UPC, Gran Capitan s/n, Modulo Cl E-08034, Barcelona, Spain.
†E-mail: miguel.cervera@upc.es

Received 14 July 2003
Revised 30 October 2003
Accepted 21 November 2003

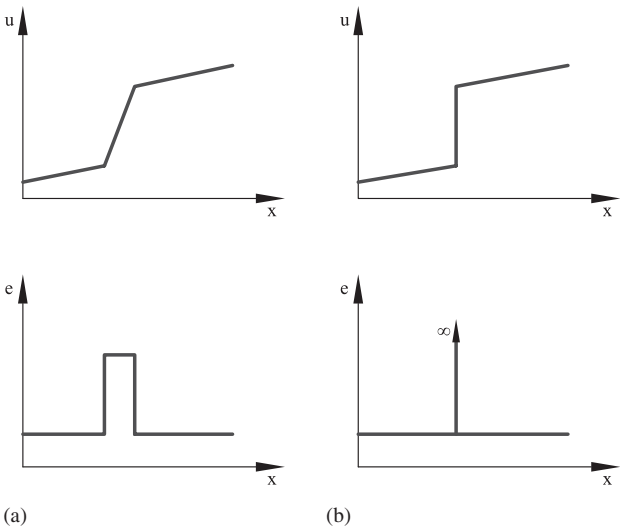

Figure 1. Strain localization: (a) weak discocntinuity; and (b) strong discontinuity.

In the last two decades, many different finite element strategies have been devised to model discontinuities and the references in the bibliography are innumerable. Two comprehensive and up-to-date overviews are given in References [1, 2]. The possibilities are several, and both the weak and the strong discontinuity approaches have been followed. In the first, the objective is to capture the localization band as precisely as possible, with standard continuous elements (see, for instance, Reference [3]). In the second, the displacement field is enhanced with discontinuous functions so that the true discontinuity line can be captured (see, for instance, Reference [4]). It is always possible to interpret a weak discontinuity as a regularization of a strong one, with the discontinuity 'smeared' across the maximum possible resolution of the mesh, that is, one element.

Remarkably, most of the studies about localization with J2 plasticity have been carried out using the irreducible formulation, with the displacement field as only unknown variable. Unfortunately, J2 plastic flow is isochoric, and the irreducible formulation is not well suited to cope with the corresponding incompressibility constraint. Even for compressible elastic materials, for localization to take place, the plastic regime has to be well developed and, then, the (incompressible) plastic part of the deformation is dominant over the (compressible) elastic part. The unsuitability of the irreductible formulation is more evident if low order finite elements are used and, very especially, for simplicial elements (triangles and tetrahedra). The need to solve this difficulty is still today the drive for active research, see, for instance, Reference [5].

On the other hand, the mixed displacement/pressure ($\mathbf{u}/p$) formulation is the appropriate framework to tackle (quasi)-incompressible problems [6]. In fact, very promising results have been obtained in localization problems with J2 plasticity using this formulation together with remeshing techniques in References [7, 8] and in coupled dynamic problems in References [9, 10]. Nevertheless, it is very difficult to construct stable low-order elements and, again, particularly, low-order simplicial elements. This is another very attractive area of on-going research, see References [11–20] among others.

Recently, the authors have applied *stabilization methods*, originated in the fluid dynamics community [21–24], to the solution of incompressible elasto-plastic problems with mixed linear/linear simplicial elements, see References [25–27]. In this paper, we extent the applicability of these stabilization procedures to the softening plastic regime, to show that results can be obtained which are free of pressure oscillations and volumetric locking and, also, which are practically *mesh independent*. This translates in the achievement of two important goals: (a) the position and orientation of the localization band is independent of the directional bias of the finite element mesh and (b) the global post-peak load–deflection curves are independent of the size of the elements in the localization band.

The accomplishment of these objectives is attained by ensuring both *global and local stability of the problem*. Global stability is necessary to preclude global wild oscillations of the pressure induced by the incompressible behaviour inside the localization band. In this work, this is secured by the modification of the standard Galerkin variational formulation, making use of the concept of sub-grid approximation. On the other hand, local stability is necessary to eliminate local oscillations in the vicinity of the band. Here, this is fulfilled by a slight modification of the global stabilization procedure, namely, making the stabilization parameter depending on the amount of plastic deformation accumulated inside the localization band. This results in a suitable stabilization technique, virtually free of spurious pressure oscillations.

The outline of the paper is as follows. In the next section, the mixed displacement/pressure ($\mathbf{u}/p$) finite element formulation for incompressible elasto-plastic behaviour is summarized. The necessary regularization of the softening modulus according to the size of the elements inside the localization band is discussed. Later, the corresponding boundary value problem is formulated. Strong and weak forms are presented and globally stabilized with the Orthogonal SubGrid Scale (OSGS) and Galerkin Least Square (GLS) methods. Also, a non-linear modification of the stabilization parameter is introduced to get rid of the local oscillations in the neighbourhood of the localization band. The possibility of enhancing the convergence of the numerical procedure by the inclusion of artificial viscosity, in a consistent fashion, is also considered. Implementation and computational aspects are discussed next. Finally, some numerical benchmarks and examples are presented to assess the present formulation and to compare its performance with the standard irreductible and mixed Galerkin triangular and tetrahedral elements.

2. MIXED FORMULATION FOR J2 PLASTICITY AND VISCOPLASTICITY

2.1. J2 plasticity and viscoplasticity

The formulation of the incompressible elasto-plastic mechanical problem can be written considering the hydrostatic pressure p as an independent unknown, additional to the primary displacement field. The stress tensor $\boldsymbol{\sigma}$ is then expressed as

$$\boldsymbol{\sigma} = p\mathbf{1} + \mathbf{s} \tag{1}$$

where $p = \frac{1}{3}\mathrm{tr}(\boldsymbol{\sigma})$ and $\mathbf{s} = \mathrm{dev}(\boldsymbol{\sigma})$ are the volumetric and the deviatoric parts of the stress tensor, respectively. Correspondingly, the strain tensor $\boldsymbol{\varepsilon} = \nabla^s\mathbf{u}$, where $\mathbf{u}$ are the displacements, is expressed as

$$\boldsymbol{\varepsilon}(\mathbf{u}) = \tfrac{1}{3}\varepsilon_v\mathbf{1} + \mathbf{e} \tag{2}$$

where $\varepsilon_v = \operatorname{tr}\boldsymbol{\varepsilon} = \nabla \cdot \mathbf{u}$ and $\mathbf{e} = \operatorname{dev}\boldsymbol{\varepsilon}$ are the volumetric and the deviatoric parts of the strain tensor, respectively. On the other hand, the constitutive equations are expressed as

$$p = K\varepsilon_v^{\mathrm{e}} \tag{3}$$

$$\mathbf{s} = 2G \operatorname{dev}\boldsymbol{\varepsilon}^{\mathrm{e}} = 2G\mathbf{e}^{\mathrm{e}} \tag{4}$$

where $\varepsilon_v^{\mathrm{e}}$ and $\mathbf{e}^{\mathrm{e}}$ are the *elastic* volumetric and the deviatoric parts of the strain tensor, respectively; K is the bulk modulus, also referred to as modulus of volumetric compressibility, and G is the shear modulus. In incompressible elasticity, K tends to infinity and, thus, $\varepsilon_v^{\mathrm{e}}$ vanishes. Additionally, in incompressible (J2) plasticity, the volumetric part of plastic deformation is zero, so that $\varepsilon_v = \varepsilon_v^{\mathrm{e}} = \nabla \cdot \mathbf{u} = 0$. On the other hand, the elastic deviatoric strain tensor $\mathbf{e}^{\mathrm{e}}$ is defined as

$$\mathbf{e}^{\mathrm{e}} = \mathbf{e} - \mathbf{e}^{\mathrm{p}} \tag{5}$$

where $\mathbf{e}^{\mathrm{p}}$ is the plastic strain tensor, which in J2 plasticity is purely deviatoric.

Box 1 summarizes the elasto-plastic model used in this work, accounting for isotropic softening. As usual, the *equivalent plastic strain* is defined as $\xi = \left(\sqrt{2/3}\right) \int_0^t \|\dot{\mathbf{e}}^{\mathrm{p}}\| \, \mathrm{d}t$, and the equivalent von Mises stress is $\bar{s} = \left(\sqrt{3/2}\right)\|\mathbf{s}\|$. With these definitions, the rate of plastic work is $\dot{\mathscr{W}}^{\mathrm{p}} = \mathbf{s} : \dot{\mathbf{e}}^{\mathrm{p}} = \bar{s}\dot{\xi}$.

Note in Box 1 that the isotropic softening variable $r = r(\xi)$ defines the current size of the yield surface, as it controls the value of the radius of the von Mises cylinder. Initially, when the equivalent plastic strain $\xi = 0, r$ is equal to the initial flow stress σ_0. Along the softening regime, r diminishes and, for large value of the equivalent plastic strain, it vanishes.

The plastic multiplier $\dot{\gamma}$ is determined from the Kuhn–Tucker and consistency conditions:

$$\dot{\gamma} \geqslant 0, \quad \Phi(\mathbf{s}, r) \leqslant 0, \quad \dot{\gamma}\Phi(\mathbf{s}, r) = 0 \tag{6a}$$

$$\text{if } \Phi(\mathbf{s}, r) = 0 \quad \text{then } \dot{\gamma}\dot{\Phi}(\mathbf{s}, r) = 0 \tag{6b}$$

The elasto-plastic model described so far can be considered as the limiting inviscid case of a rate-dependent J2 elasto-viscoplastic model. The *only* formal difference between visco-plasticity and inviscid plasticity is that in the viscous case the Kuhn–Tucker and consistency conditions are replaced by an explicit evolution law for the plastic multiplier $\dot{\gamma}$, for instance in the form

$$\dot{\gamma} = \left\langle \frac{\Phi}{\eta} \right\rangle^m \tag{7}$$

where η is the viscosity and m is a viscosity exponent. Note that for very low values of the viscosity, $\eta \to 0$, or very small relaxation times, $\bar{\tau} := \eta/G$, the inviscid plastic model is recovered.

Details on how to integrate along time both the elasto-plastic and the elasto-viscoplastic constitutive models can be found in Reference [28]. As it will be explained later, it is often advantageous to use a *consistent viscous regularization* of the plastic case to be able to obtain solutions for the inviscid case in a robust and efficient way.

2.2. Softening behaviour

Either considering linear or exponential softening, the elasto-plastic model described above is able to reproduce the softening branch that occurs in a test under monotonic straining after the

peak stress is reached, with the stress decreasing asymptotically to the strain axis. With such behaviour, a finite area is retained between the stress–strain curve and the strain axis. This area defines the available energy to be dissipated in the control volume. When modelling weak discontinuities (or regularized strong discontinuities) with finite elements, this energy has to be appropriately related to the fracture energy of the material, G_f, to satisfy the requisites of mesh-size objectivity. This is accomplished by the introduction of a geometrical factor, l_{ch}, called *characteristic length*, which depends on the spatial discretization and ensures conservation of the energy dissipated by the material upon mesh-size refinements [3]. Accordingly, the determination of the softening parameter H_S is made by equating the material fracture energy *per unit of characteristic length* to the total dissipation along the deformation process.

For the elasto-plastic model, the rate of plastic work can be computed as

$$\dot{\mathscr{W}}^p = \mathbf{s} : \dot{\mathbf{e}}^p = \bar{s}\dot{\xi} = r(\xi)\dot{\xi} \tag{8}$$

Thus, the total plastic work along a process with softening is

$$\mathscr{W}^p = \int_{t=0}^{t=\infty} \dot{\mathscr{W}}^p \, dt = \int_{\xi=0}^{\xi=\infty} r(\xi)\dot{\xi} = \frac{\sigma_0^2}{2H_S} \tag{9}$$

It has to be remarked that the total plastic work is equal to the 'area' below the $r - \xi$ curve, that defines the softening response. Also, note that the result in Equation (9) holds both for linear and exponential softening, due to the appropriate definition of these in Box 1.

Box 1. J2-plastic constitutive model

(1) Von Mises yield function, Φ:

$$\Phi(\mathbf{s}, r) = \sqrt{\tfrac{3}{2}}\|\mathbf{s}\| - r = \bar{s} - r$$

(2) Isotropic softening variable, r:

$$r = \begin{cases} \sigma_0\left(1 - \dfrac{H_S}{\sigma_0}\xi\right) & 0 \leqslant \xi \leqslant \dfrac{\sigma_0}{H_S} \\ 0 & \dfrac{\sigma_0}{H_S} \leqslant \xi \leqslant \infty \end{cases} \quad \text{linear softening}$$

$$r = \sigma_0 \exp\left(-\frac{2H_S}{\sigma_0}\xi\right) \quad 0 \leqslant \xi \leqslant \infty \quad \text{exponential soft.}$$

where ξ is the equivalent plastic strain, σ_0 is the flow stress and $H_S > 0$ is the softening coefficient.

(3) Plastic evolution laws:

$$\dot{\mathbf{e}}^p = \dot{\gamma}\,\mathbf{n}$$

$$\dot{\xi} = \dot{\gamma}\sqrt{\tfrac{2}{3}}$$

where $\dot{\gamma}$ is the plastic multiplier and $\mathbf{n} = \dfrac{\partial \Phi}{\partial \mathbf{s}} = \dfrac{\mathbf{s}}{\|\mathbf{s}\|}$ is the normal to the yield surface.

Equating the total plastic work to the energy (per unit volume) to be dissipated in the localization band, $\mathscr{W}^{\mathrm{p}} = G_{\mathrm{f}}/l_{\mathrm{ch}}$, it yields

$$H_{\mathrm{S}} = \frac{\sigma_0^2}{2G_{\mathrm{f}}}\, l_{\mathrm{ch}} = \bar{H}_{\mathrm{S}} l_{\mathrm{ch}} \tag{10}$$

where $\bar{H}_{\mathrm{S}}$ only depends on the material properties. This is consistent with the results obtained in the strong discontinuity approach [4]. For linear elements, the characteristic length can be taken as the representative size of the element, $l_{\mathrm{ch}} = h_e$. In this work, the size of the element will be computed as $h_e^2 = 2A_e$ for triangular elements and $h_e^2 = A_e$ for quadrilateral elements, A_e being the area of the element. In 3D applications, $h_e^3 = 6V_e$ for tetrahedral elements and $h_e^3 = V_e$ for hexahedral elements, where V_e is the volume of the element.

3. BOUNDARY VALUE PROBLEM

3.1. Strong and weak forms

The strong form of the continuum mechanical problem can be stated as: find the displacement field $\mathbf{u}$ and the pressure field p, for given prescribed body forces $\mathbf{f}$, such that

$$\nabla \cdot \mathbf{s} + \nabla p + \mathbf{f} = \mathbf{0} \quad \text{in } \Omega \tag{11}$$

$$\nabla \cdot \mathbf{u} - \frac{1}{K}\, p = 0 \quad \text{in } \Omega \tag{12}$$

where Ω is the open and bounded domain of $\mathbb{R}^{n_{\mathrm{dim}}}$ occupied by the elasto-plastic solid in a space of n_{dim} dimensions. Equations (11)–(12) are subjected to appropriate Diritchlet and Neumann boundary conditions. In the following, we will assume these in the form of prescribed displacements $\mathbf{u} = \bar{\mathbf{u}}$ on $\partial\Omega_u$, and prescribed tractions $\bar{\mathbf{t}}$ on $\partial\Omega_t$, respectively. In the mixed formulation, the value of the pressure is defined by the Neumann conditions or, alternatively, by prescribing its value at some point.

The associated weak form of problem (11) + (12) can be stated as

$$(\mathbf{v}, \nabla \cdot \mathbf{s}) + (\mathbf{v}, \nabla p) + (\mathbf{v}, \mathbf{f}) = 0 \quad \forall \mathbf{v} \tag{13}$$

$$(q, \nabla \cdot \mathbf{u}) - \left(q, \frac{1}{K}\, p\right) = 0 \quad \forall q \tag{14}$$

where $\mathbf{v} \in \mathscr{V}$ and $q \in \mathscr{Q}$ are the variations of the displacements and pressure fields, respectively, and $(\cdot\,,\cdot)$ denotes the inner product in $L^2(\Omega)$, the space of square integrable functions in Ω. Integrating Equation (13) by parts, the problem can be rewritten in the standard form as

$$(\nabla^s \mathbf{v}, \mathbf{s}) + (\nabla \cdot \mathbf{v}, p) - (\mathbf{v}, \mathbf{f}) - (\mathbf{v}, \bar{\mathbf{t}})_{\partial\Omega_t} = 0 \quad \forall \mathbf{v} \tag{15}$$

$$(q, \nabla \cdot \mathbf{u}) - \left(q, \frac{1}{K}\, p\right) = 0 \quad \forall q \tag{16}$$

3.2. Discrete form. Global stabilization techniques

The *discrete* finite element form of the problem is obtained from Equations (15)–(16), substituting the displacement and pressure fields and their variations by their standard finite

element interpolations:

$$(\nabla^s \mathbf{v}_h, \mathbf{s}_h) + (\nabla \cdot \mathbf{v}_h, p_h) - (\mathbf{v}_h, \mathbf{f}) - (\mathbf{v}_h, \bar{\mathbf{t}})_{\partial\Omega_t} = 0 \quad \forall \mathbf{v}_h \tag{17}$$

$$(q_h, \nabla \cdot \mathbf{u}_h) - \left(q_h, \frac{1}{K} p_h\right) = 0 \quad \forall q_h \tag{18}$$

where $\mathbf{u}_h, \mathbf{v}_h \in \mathscr{V}_h$ and $p_h, q_h \in \mathscr{Q}_h$ are the *discrete* displacement and pressure fields and their variations, defined onto the finite element spaces $\mathscr{V}_h$ and $\mathscr{Q}_h$, respectively. As it is well known, the BB-condition [29] poses severe restrictions on the choice of the spaces $\mathscr{V}_h$ and $\mathscr{Q}_h$ when using the standard Galerkin discrete form (17)–(18). For instance, standard mixed elements with continuous equal order linear/linear interpolation for both fields are not stable, and the lack of stability shows as uncontrollable oscillations in the pressure field that usually, and very particularly in non-linear problems, pollute the solution entirely. Fortunately, the strictness of the BB-condition can be circumvented by modifying the discrete variational form appropriately, in order to attain the necessary global stability with the desired choice of interpolation spaces.

One way of 'expanding' the choice of interpolation spaces comes from the sub-grid scale approach, firstly proposed in Reference [21]. The concept was further exploited in Reference [24], where the concept of *orthogonal* sub-scales was introduced and, thereafter, successfully applied to several fluid dynamics problems. Application of the orthogonal sub-grid scale stabilization method (OSGS) to the problem of incompressible elasto-plasticity has been formulated by the authors in previous works and the interested reader is referred to them for a detailed explanation, see References [25–27].

The basic idea is to 'enhance' the approximation of the discrete displacements provided from the 'coarse' finite element grid with *the stabilization effect* of a finer 'sub-grid' scale. The displacements of the sub-scale are thought of as a perturbation of the ones resolved by the finite element scale. By definition, this sub-grid component cannot be resolved by the computational grid, but appropriate approximations can be introduced in order to account for its desired effects. With these approximations it is possible to arrive to the following form of the modified *stabilized discrete problem*:

$$(\nabla^s \mathbf{v}_h, \mathbf{s}_h) + (\nabla \cdot \mathbf{v}_h, p_h) - (\mathbf{v}_h, \mathbf{f}) - (\mathbf{v}_h, \bar{\mathbf{t}})_{\partial\Omega_t} = 0 \quad \forall \mathbf{v}_h \tag{19}$$

$$(q_h, \nabla \cdot \mathbf{u}_h) - \left(q_h, \frac{1}{K} p_h\right) - \boxed{\sum_{e=1}^{n_{\text{elm}}} \tau_e (\nabla q_h \cdot [\nabla p_h - \boldsymbol{\Pi}_h])} = 0 \quad \forall q_h \tag{20}$$

$$(\nabla p_h, \boldsymbol{\eta}_h) - (\boldsymbol{\Pi}_h, \boldsymbol{\eta}_h) = 0 \quad \forall \boldsymbol{\eta}_h \tag{21}$$

where the stabilization parameter $\tau_e = \mathrm{ch}_e^2/2G$ is defined as a function of the characteristic length of the element h_e and the shear modulus G. The constant $c = \mathscr{O}(1)$ has to be determined through numerical testing.

It is important to point out that, when using linear/linear displacement and pressure interpolations, with this approach no stabilization term appears in the momentum balance equation (19), which can be solved as in a standard mixed finite element formulation. The only stabilization term appears in the incompressibility equation (20). Observe that in it, a third nodal variable $\boldsymbol{\Pi}_h$ is involved. As can be seen in Equation (21), this is not other that the L_2–projection (least-square fitting) of the pressure gradient, $\boldsymbol{\Pi}_h = P_h(\nabla p_h)$. The next section

shows that the drawback of accounting for an extra nodal variable can be easily overcome to achieve a robust and efficient procedure.

It is obvious in Equation (20) that the effect of the stabilization technique is to add a term that relaxes the strict quasi-incompressibility constraint posed by this equation. Note that this relaxation is very small, as $\tau_e = \mathcal{O}(h^2)$ and it depends on the difference between the discontinuous pressure gradient and its continuous least square projection. This difference tends to vanish as the mesh is refined.

An alternative, somewhat simpler, stabilization method is the one known as GLS, originally proposed in References [30, 31], and used in solid mechanics in Reference [13] to solve finite strain elasticity problems. The corresponding *stabilized discrete problem* reads

$$(\nabla^s \mathbf{v}_h, \mathbf{s}_h) + (\nabla \cdot \mathbf{v}_h, p_h) - (\mathbf{v}_h, \mathbf{f}) - (\mathbf{v}_h, \bar{\mathbf{t}})_{\partial\Omega_t} = 0 \quad \forall \mathbf{v}_h \tag{22}$$

$$(q_h, \nabla \cdot \mathbf{u}_h) - \left(q_h, \frac{1}{K} p_h\right) - \boxed{\sum_{e=1}^{n_{\text{elm}}} \tau_e (\nabla q_h \cdot \nabla p_h)} = 0 \quad \forall q_h \tag{23}$$

which has a format very similar to the OSGS method, but does not require the computation of any extra nodal variable. Experience shows that the GLS method is more 'diffusive' than the OSGS stabilization. This means that GLS is somewhat more 'robust' than OSGS, but sometimes less sharp localizations are obtained.

3.3. Local stabilization

The global stabilization techniques discussed in the previous section are designed to provide global stability to the incompressible elasto-plastic problem. In the cases of elastic incompressibility or smooth widespread, non-localizing, plastic responses, they are able to preclude the pressure oscillations that arise if the standard Galerkin method is used (see References [25, 26]). In Reference [27] it was found that, with perfect plasticity, the stabilization parameter has to be modified to account for the development of the plastic regime, as deformation localizes into weak discontinuities; otherwise, pressure oscillations arise in the vicinity of the plastic areas and pollute the solution.

In Reference [27], it was proposed to enhance the stabilization properties using a *non-linear* stabilization parameter, $\tau_e = ch_e^2/2G^*$, computed as a function of the characteristic length of the element h_e and the current *secant* shear modulus G^*, defined as (half) the ratio between the norms of the deviatoric stress and *total* strain tensors, $2G^* = \|\mathbf{s}_h\|/\|\mathbf{e}_h\|$. For plasticity, this ratio is obviously non-constant and it varies along the deformation process. It is clear that, as plastic deformation evolves, the ratio G^*/G decreases and, consequently, the value of τ_e increases, further relaxing the incompressibility constraint imposed by the isochoric nature of the plastic flow.

3.4. Consistent residual viscosity

For softening materials, strain localizes and the ratio G^*/G decreases very fast with plastic deformation and, ultimately, vanishes, yielding very large values of the stabilization parameter. In many practical applications, it is found that this almost unbounded increase of the stabilization term causes numerical difficulties that translate in slow or even lack of convergence

of the solution of the non-linear process, particularly in problems involving singular points, where the strains reach very high values in early stages of the analysis.

One obvious way to alleviate this difficulty is to define an *ad hoc* cut-off for the decrease of the values of the secant modulus G^* or, alternatively, on the increase of the values of the stabilization parameter τ_e. Unfortunately, experience shows that this leads to the impossibility of the total elimination of the local oscillations of the pressure. The greater the value of the cut-off, the better is the convergence, but greater are the remaining local pressure oscillations.

Therefore, a different approach is preferred to enhance the convergence of the non-linear equilibrium iterations. This consists in introducing a viscous regularization of the plastic model, transforming it in (slightly) viscoplastic. The numerical benefits of this viscous regularization are well known and documented in the literature, but it is also true that the addition of 'artificial' viscosity in an indiscriminate fashion rather changes the nature of the obtained solution. It is far more elegant to devise a high-order scheme where the minimal amount of artificial viscosity is added only where it is needed and, also, in a consistent manner, that is, with smaller values for decreasing element sizes.

It is here proposed to regularize the elasto-plastic constitutive model with an artificial viscosity defined in terms of the normal proyection of the residual of the momentum equation onto the finite element space (see Reference [27]), in the form

$$\eta = c' h_e \Delta t \| \nabla p_h - \mathbf{\Pi}_h \| \tag{24}$$

where c' is a constant, h_e is the characteristic length of the element and Δt is the time step size. Note that this viscosity acts only in those elements where the momentum equation is not exactly satisfied and that, for linear simplex, it is $\eta = \mathcal{O}(h_e^2 \Delta t)$. This means that it maintains the order of the finite element approximation, as it vanishes upon mesh (and time increment) refinement with the appropriate rate.

The structure of expression (24) suggests that it is also possible to define the viscosity purely in terms of the norm of the pressure gradient, in the form

$$\eta = c' h_e \Delta t \| \nabla p_h \| \tag{25}$$

This second proposal is consistent with the definition of the stabilization term used in the GLS method.

4. IMPLEMENTATION AND COMPUTATIONAL ASPECTS

Owing to the non-linear dependence of the stresses on the displacements, the solution of the system of equations (19)–(21) requires the use of an appropriate incremental/iterative procedure such as the Newton–Raphson method. Within such a procedure, the system of linear equations to be solved for the $(i+1)$th equilibrium iteration of the $(n+1)$th time (or load) step is

$$\begin{bmatrix} \mathbf{K}_{\text{dev}} & \mathbf{G} & \mathbf{0} \\ \mathbf{G}^{\mathrm{T}} & -\left(\dfrac{1}{K}\mathbf{M} + \mathbf{L}_{\tau}\right) & \mathbf{G}_{\tau}^{\mathrm{T}} \\ \mathbf{0} & \mathbf{G}_{\tau} & -\mathbf{M}_{\tau} \end{bmatrix}^{(n+1,i)} \begin{bmatrix} \delta\mathbf{U} \\ \delta\mathbf{P} \\ \delta\mathbf{\Pi} \end{bmatrix}^{(n+1,i+1)} = -\begin{bmatrix} \mathbf{R}_1 \\ \mathbf{R}_2 \\ \mathbf{0} \end{bmatrix}^{(n+1,i)} \tag{26}$$

where $\delta\mathbf{U}, \delta\mathbf{P}$ and $\delta\mathbf{\Pi}$ are the iterative corrections to the nodal values for the displacements, pressure and pressure gradient, respectively, $\mathbf{R}_1$ and $\mathbf{R}_2$ are the residual vectors associated to the

satisfaction of the balance of momentum and incompressibility equations, respectively, and the *global* matrices $\mathbf{K}_{\text{dev}}, \mathbf{G}, \mathbf{G}_\tau, \mathbf{M}, \mathbf{L}_\tau$ and $\mathbf{M}_\tau$ come from the standard assembly procedure of the elemental contributions, for the ith iteration of the $n+1$ step. Note that this global matrix is symmetric, but it is not positive definite.

The monolithic solution of system (26) can be avoided by using a staggered procedure, in which the pressure projection $\mathbf{\Pi}^{(n+1,i+1)}$ is solved independently and explicitly. To this end, from the third equation, it is possible to express $\mathbf{\Pi}^{(n+1,i+1)}$ in terms of $\mathbf{P}^{(n+1,i+1)}$ as

$$\mathbf{\Pi}^{(n+1,i+1)} = (\mathbf{M}_\tau^{-1})^{(n+1,i)} \mathbf{G}_\tau^{(n+1,i)} \mathbf{P}^{(n+1,i+1)} \cong \bar{\mathbf{M}}^{-1} \mathbf{G} \mathbf{P}^{(n+1,i+1)} \tag{27}$$

The computation of the projections $\mathbf{\Pi}$ can be transformed in a straight-forward operation by neglecting the difference in the τ_e coefficient in adjacent elements and considering an approximate lumped mass matrix $\bar{\mathbf{M}}$.

One further approximation can be introduced to make the solution of the mixed system of equations more efficient from the computational point of view. This consists in keeping the projected pressure gradient constant during the equilibrium iterations within each time increment, taking it equal to the corresponding value at the end of the previous time step, that is $\mathbf{\Pi}^{(n+1,i+1)} \cong \mathbf{\Pi}^{(n)}$. This strategy has proved effective without loss of precision nor robustness.

From the above, the implementation of the GLS method is straight-forward; it is enough to delete the third equation in (26), together with the corresponding third column of the global matrix, to yield

$$\begin{bmatrix} \mathbf{K}_{\text{dev}} & \mathbf{G} \\ \mathbf{G}^{\mathrm{T}} & -\left(\dfrac{1}{K}\mathbf{M} + \mathbf{L}_\tau\right) \end{bmatrix}^{(n+1,i)} \begin{bmatrix} \delta\mathbf{U} \\ \delta\mathbf{P} \end{bmatrix}^{(n+1,i+1)} = -\begin{bmatrix} \mathbf{R}_1 \\ \mathbf{R}_2 \end{bmatrix}^{(n+1,i)} \tag{28}$$

where the effect of the stabilization matrix $\mathbf{L}_\tau$ is evident. For the OSGS, the stabilization matrix can be formally expressed as $\hat{\mathbf{L}}_\tau = \mathbf{L}_\tau - \mathbf{G}_\tau^{\mathrm{T}} \mathbf{M}_\tau^{-1} \mathbf{G}_\tau$.

5. NUMERICAL RESULTS

The formulation presented in the preceding sections is illustrated below in a number of benchmark problems. Performance of the global and local stabilization method is tested considering 2D plane-strain triangular meshes and 3D tetrahedral meshes. The examples involve both *compressible* and *incompressible* elasticity and J2-plasticity with exponential *softening*. The following material properties are assumed: Young's modulus $E = 10$ MPa, different Poisson's ratios (recall that $G = E/2(1+\nu)$, $K = E/3(1-2\nu)$), yield stress $\sigma_0 = E/1000 = 10$ KPa and different fracture energies. A value $c = 1$ is taken for the evaluation of τ_e. Values in the range $c' = 10$–100 are used for the evaluation of the viscous regularization.

The Newton–Raphson method, combined with a line search procedure is used to solve the non-linear system of equations arising from the spatial and temporal discretization of the weak form of the stabilized problem. In all cases 200 equal time steps are performed to complete the analyses. Calculations are performed with an enhanced version of the finite element program COMET [32], developed by the authors at the International Center for Numerical Methods in Engineering (CIMNE). Pre- and post-processing is done with GiD, also developed at CIMNE [33].

5.1. 2D Perforated strip

The first example is a plane-strain perforated strip loaded through a rigid platen which sustains an axial central point load. Owing to the double symmetry, only one quarter of the domain (the top right quarter) needs to be discretized. Figure 2(a) depicts the geometry of the problem; dimensions are related to length $r = 1$ m. Figure 2 also shows two of the three unstructured meshes used in the analyses: (b) a coarse mesh of 438 linear triangles (251 nodes), (c) a medium mesh of 1,903 linear triangles (1,020 nodes), and (not shown) a fine mesh of 7,489 linear triangles (3,880 nodes). Note that in all the unstructured meshes the pre-processor used tends to introduce patches or equilateral triangles with predominant directions at -30°, $+30^\circ$ and $+90^\circ$.

For this example, a Poisson ratio $\nu = 0.3$ is used and, therefore, compressible elasticity is assumed; fracture energy is $G_f = 200\ \mathrm{J/m^2}$ (which corresponds to a softening parameter $\bar{H}_S = 0.25$ MPa/m). The value $c' = 10$ is used for the evaluation of the viscous regularization.

Figure 3 shows (half)-load vs. ((half)-imposed point of application)–displacement curves (1 m thickness is assumed) obtained with different formulations: (a) standard irreductible **u** (3-noded CST with linear continuous displacement field), (b) standard mixed **u**/p (3-noded triangles with linear continuous displacement and pressure fields), (c) mixed **u**/p with global OSGS stabilization, (d) mixed **u**/p with global and local OSGS stabilization and (e) mixed **u**/p with global and local GLS stabilization. The corresponding analyses are run using the medium mesh depicted in Figure 2(c). Several remarks are in order. First, all the mixed formulations capture reasonably well both the limit load and the general softening trend of the curve, while the irreductible formulation fails to do so almost completely. Second, the effect of the stabilization techniques adopted is obvious in the global softening response, with clear advantage for the global and local method over the purely global one. Third, the difference between the OSGS and the GLS methods is small. As it will be seen below, the differences in the responses are due to the

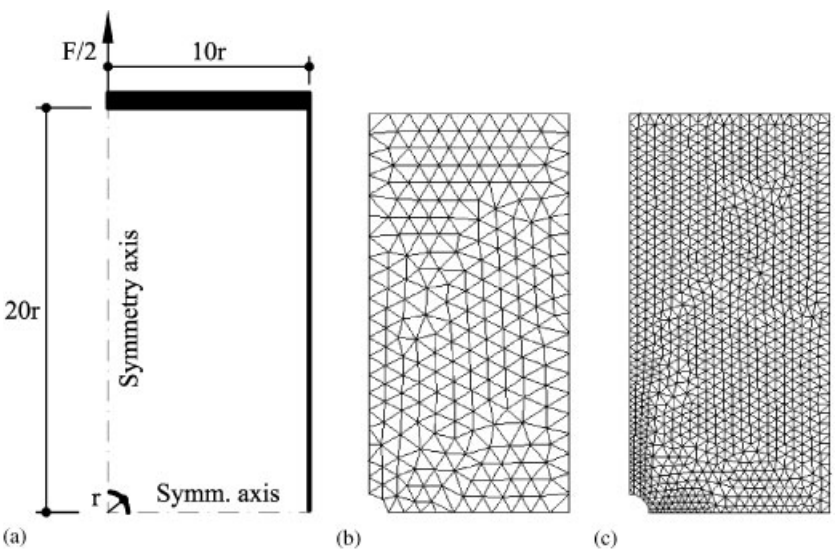

Figure 2. Geometry and meshes for the 2D perforated strip: (a) geometry; (b) coarse mesh; and (c) medium mesh.

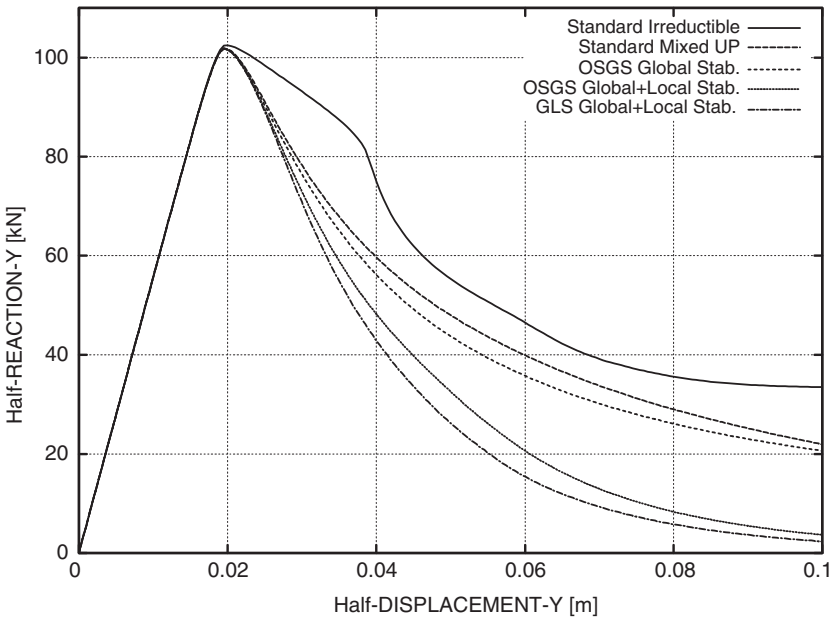

Figure 3. (Half)-load vs. (half)–imposed displacement curve for 2D perforated strip using different formulations.

different degrees of success of the formulations in removing the volumetric locking induced by the development of the plastic behaviour.

Figures 4 and 5 depict the deformed shape and contours of the effective plastic strain once the plastic flow is fully developed and the collapse mechanism can be appreciated (vertical displacement of the load $\delta = 0.1$ m), both for the irreductible and the stabilized mixed formulations. On one hand, Figure 4 shows results for the irreductible formulation. Note how the localization band forms an angle of $+30^\circ$ with the horizontal axis and it is completely influenced by the directional bias of the mesh.

Correspondingly, Figure 5 shows results for the stabilized mixed formulation. Here, the localization band forms a correct angle of approximately $+45^\circ$ with the horizontal axis and it is virtually free on any directional bias from the mesh. Also, note that the resolution of the shear band is optimal, as it is only one element across.

It has to be remarked that the deformation pattern and collapse mechanism predicted by all the mixed formulations are practically identical, independently of the stabilization method used, or even if no stabilization is introduced. Therefore, the ability of the mixed formulation to capture the correct plastic localization pattern is demonstrated.

Figure 6 presents pressure contours at the same time (final) of the deformation process. Lack of stability and severe oscillations of the pressure field can be identified in *both* the irreductible (a) and mixed (b) standard formulations. This is enough to completely destabilize the irreductible formulation, although for this example it seems to have little influence in the deformation pattern of the mixed formulation, as the plastic deformation does not depend on the actual values of the pressure. Obviously, this is not always necessarily the case, and especially in non-linear analyses. Also, the improved performance of the stabilized formulations

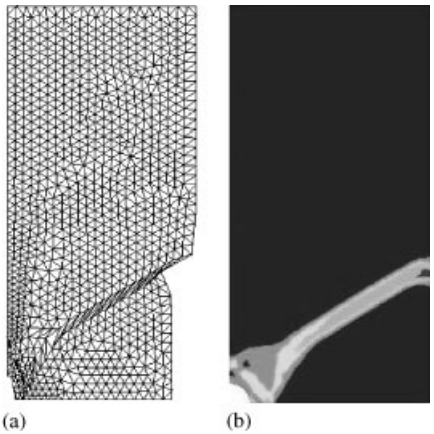

Figure 4. Deformed shape and equivalent plastic strain contour fills for the 2D perforated strip with irreductible formulation.

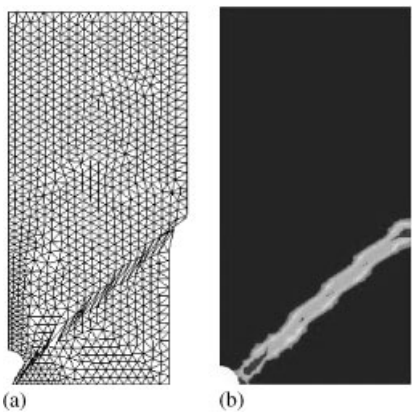

Figure 5. Deformed shape and equivalent plastic strain contour fills for the 2D perforated strip with stabilized mixed formulation.

is easily perceptible. Note that if a linear stabilization term is used, (c), only global stability is achieved and pressure oscillations are still visible in the vicinity of the localization band, both along and across the direction of the slip. This oscillations are completely removed from Figure (d), where the non-linear stabilization parameter is used, achieving both global and local stabilization of the pressure field.

Finally, Figure 7 shows (half)-load vs. ((half)-imposed point of application)–displacement curves (1 m thickness is assumed) obtained with different unstructured meshes: (a) coarse, (b) medium and (c) fine. Note that the overall global response is satisfactorily convergent upon mesh refinement, with the total area under the load–displacement curve converging to the correct amount of plastic work dissipated to create the localization band. No spurious brittleness is observed when the size of the elements is reduced. This is achieved by the regularization procedure explained in Section 2.2.

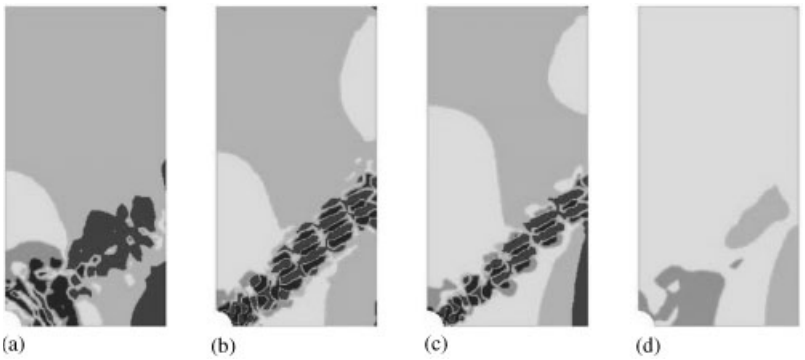

Figure 6. Pressure contour fills for the 2D perforated strip with different formulations: (a) irreductible; (b) standard mixed; (c) OSGS with global stabilization; and (d) OSGS with global and local stabilization

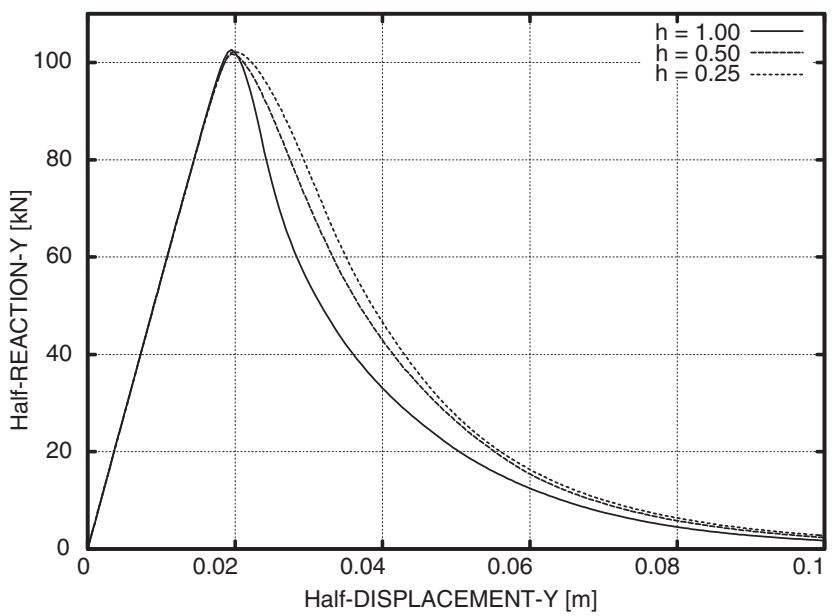

Figure 7. (Half)-load vs. (half)–imposed displacement curve for 2D perforated using different meshes.

5.2. 2D Prandtl's punch test

The second example is the Prandtl's punch test, a well-known plane-strain 2D problem often used in the literature to test the ability of J2-plastic models to capture collapse loads and mechanisms. Figure 8(a) depicts the geometry of the problem, a rigid footing with a central point load; dimensions are related to length $b = 0.5$ m.

The elastic behaviour is assumed to be incompressible and, therefore, a Poisson ratio $v = 0.5$ is used in the analyses. Nevertheless, when using the irreductible formulation a reduced value $v = 0.45$ had to be used to obtain results, even if they were very inaccurate. Fracture energy is

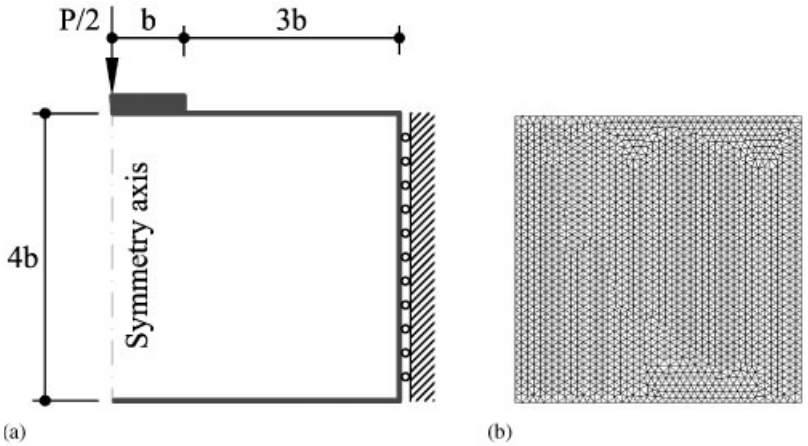

Figure 8. Geometry (a) and mesh (b) used for the 2D Prandtl's punch test.

$G_f = 50\ \mathrm{J/m^2}$ (which corresponds to a softening parameter $\bar{H}_S = 1\ \mathrm{MPa/m}$). The value $c' = 100$ is used for the evaluation of the viscous regularization.

Owing to the symmetry, only half of the domain (the right half) needs to be discretized. The mesh used in the computations is shown in Figure 8(b), unstructured with 3,624 linear triangles and 1,893 nodes. It has to be remarked that experience, and the previous example, show that localization problems require the use of much finer meshes than those necessary for problems were displacements and strains do not localize.

Figure 9 shows (half)-load vs. (point of application)–displacement curves (1 m thickness is assumed) obtained with different formulations: (a) standard irreductible **u** (3-noded CST with linear continuous displacement field), (b) standard mixed **u**/p (3-noded triangles with linear continuous displacement and pressure fields), (c) mixed **u**/p with global OSGS stabilization, (d) mixed **u**/p with global and local OSGS stabilization and (e) mixed **u**/p with global and local GLS stabilization. The results confirm the observations of the previous example: the irreductible formulation locks almost completely, while the other three formulations yield meaningful softening curves. Again, as it will be seen below, the differences in the mixed responses are due to the variable degrees of success of the various formulations in removing the volumetric locking induced by the plastic behaviour.

Figures 10 and 11 depict the deformed shape and contours of the effective plastic strain once the plastic flow is fully developed and the collapse mechanism can be appreciated (vertical displacement of the load $\delta = 0.05$ m), both for the irreductible and the stabilized mixed formulations. On one hand, Figure 10 shows results for the irreductible formulation. Note how the collapse mechanism is completely influenced by the directional bias of the mesh, with slip bands that follow exactly the predominant mesh orientations at -30°, $+30^\circ$ and $+90^\circ$. Also, spurious localization branches appear.

Correspondingly, Figure 11 shows results for the stabilized mixed formulation. Note how here, the localization bands form according to the well-known classical solution (for rigid-perfectly plastic behaviour) and it is virtually free on any directional bias from the mesh. It is particularly remarkable how the expected logarithmic spiral branch, with no spurious branching, is obtained. As in the previous example, the resolution of the shear band is optimal,

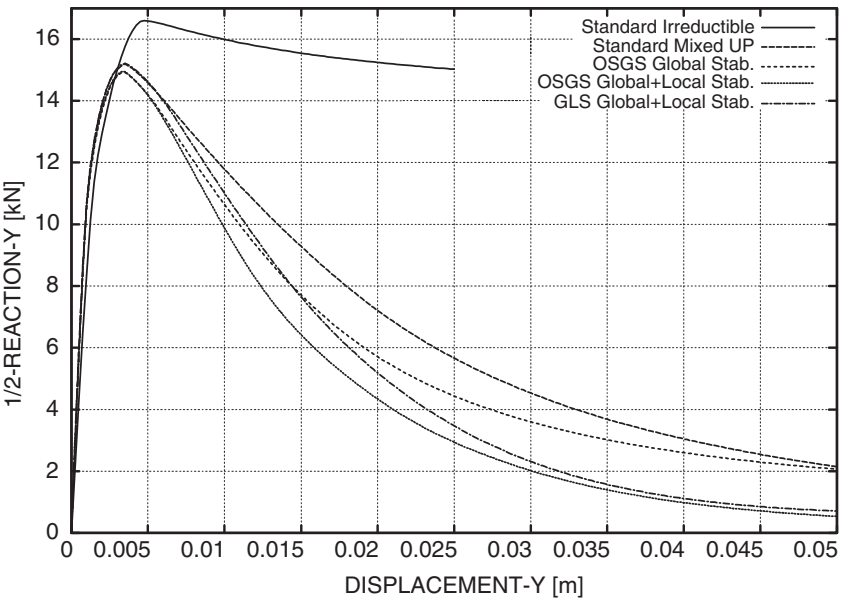

Figure 9. (Half)-load–displacement curve for 2D Prandtl's punch test.

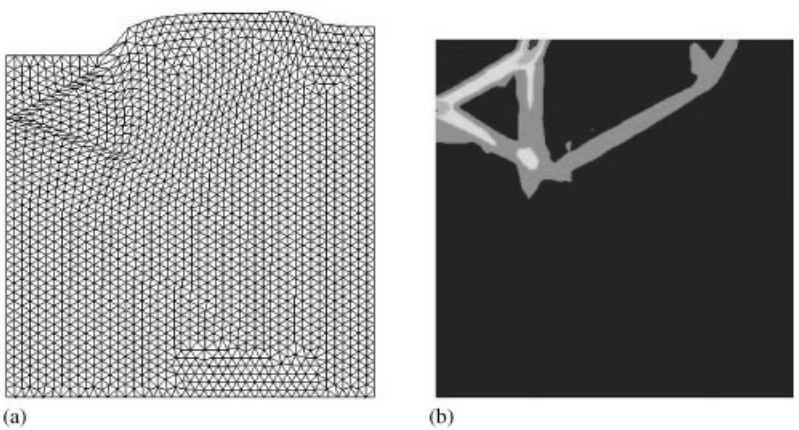

Figure 10. Deformed shape and equivalent plastic strain contour fills for the 2D perforated strip with irreductible formulation.

only one element across. Again, the deformation pattern and collapse mechanism predicted by all the mixed formulations are practically identical, independently of the stabilization method used, which demonstrates the superiority of the mixed formulation for capturing the correct plastic localization pattern.

Finally, Figure 12 presents pressure contours at the same time (final) of the deformation process, where the serious deficiencies of the standard formulations and the huge improvement achieved with a proper stabilization are evident. Note again how the proposed stabilization

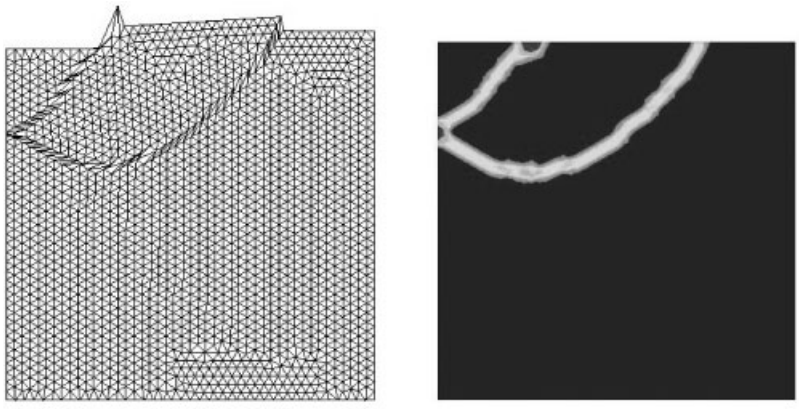

Figure 11. Deformed shape and equivalent plastic strain contour fills for the 2D perforated strip with stabilized mixed formulation.

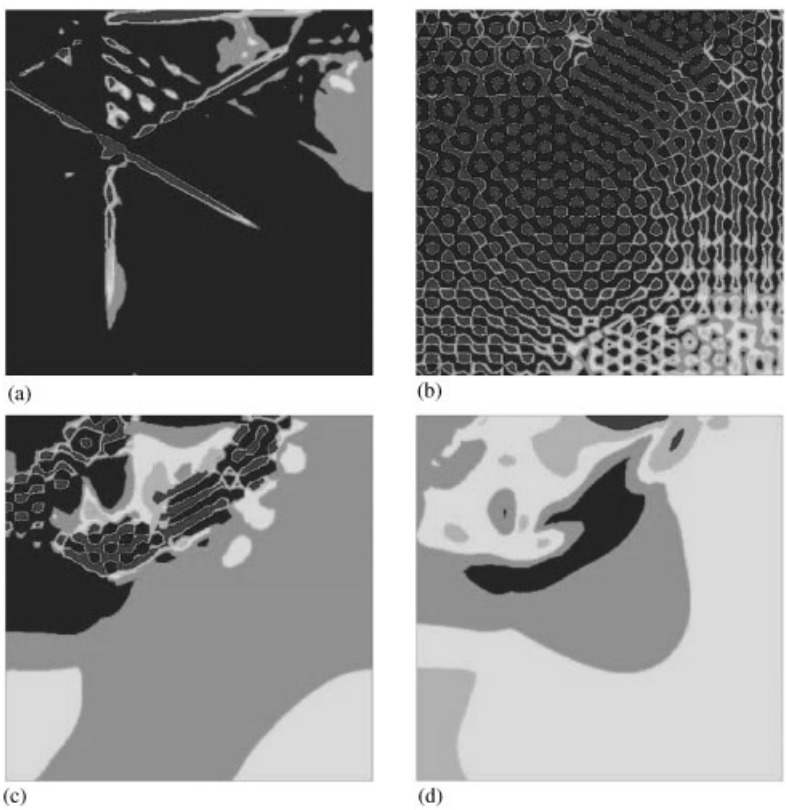

Figure 12. Pressure contour fills for the 2D perforated strip with different formulations: (a) irreductible; (b) standard mixed; (c) OSGS with global stabilization; and (d) OSGS with global and local stabilization.

technique in able to eliminate completely the pressure oscillations, including those in the vicinity of the slip bands.

5.3. 3D Prandtl's punch test

A 3D version of the previous problem is presented next. Figure 13 shows the unstructured mesh of 4-noded linear tetrahedra used in the computations (56,514 elements, 10,969 nodes). The thickness discretized is $b = 0.5$ m. Note that the element sizes in the mesh are non-uniform, but the size of the element used in the part where the localization bands are expected to form is approximately the same used in the 2D mesh in the previous section. Roller supports are prescribed in the nodes on the frontal and rear faces to simulate plane strain conditions.

Figure 14 shows the (half)-load vs. (point of application)–displacement curves obtained for the 2D and 3D cases, using the mixed $\mathbf{u}/p$ formulation with GLS global and local stabilization. It is remarkable that both cases yield such comparable results. The difference is attributed to the unstructured nature of the mesh in the transverse direction; this produces slip surfaces which are 'rough' (and not perfectly cylindrical) in the transverse direction and, therefore, the plastic work developed is greater than in the 2D case. The results (not shown) obtained with the OSGS stabilization method also compare satisfactorily with the corresponding 2D case.

Figure 15(a) displays contours of the effective plastic strain once the plastic flow is fully developed (vertical displacement of the load $\delta = 0.05$ m). This figure matches closely the results obtained in the 2D case, depicted in Figure 11. It is therefore demonstrated that the proposed formulation can capture correctly the displacement and strain localization leading to the collapse mechanism even in a 3D setting.

Finally, Figure 15(b) shows the pressure contours at the same time (final) of the deformation process. Again, it is remarkable that completely satisfactory results are obtained with the proposed formulation in an unstructured mesh of tetrahedra, very similar to those obtained in the 2D simulation.

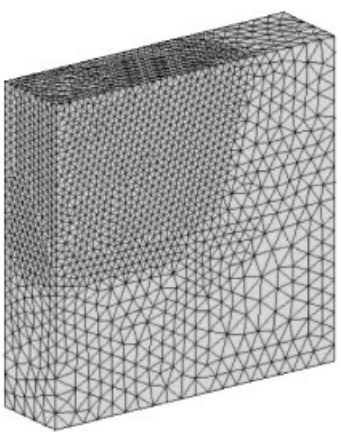

Figure 13. Unstructured mesh used for 3D Prandtl's punch test.

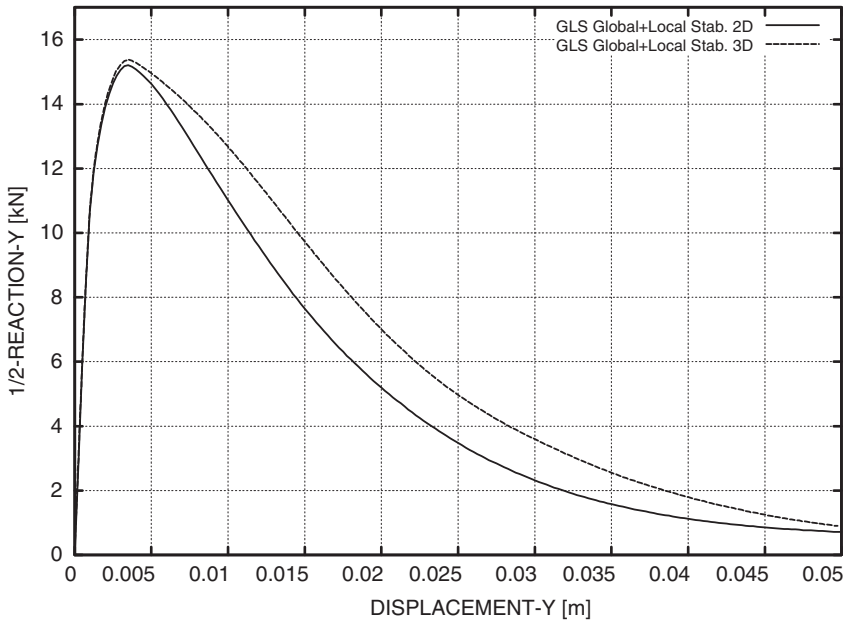

Figure 14. (Half)-load–displacement curve for 2D and 3D Prandtl's punch test.

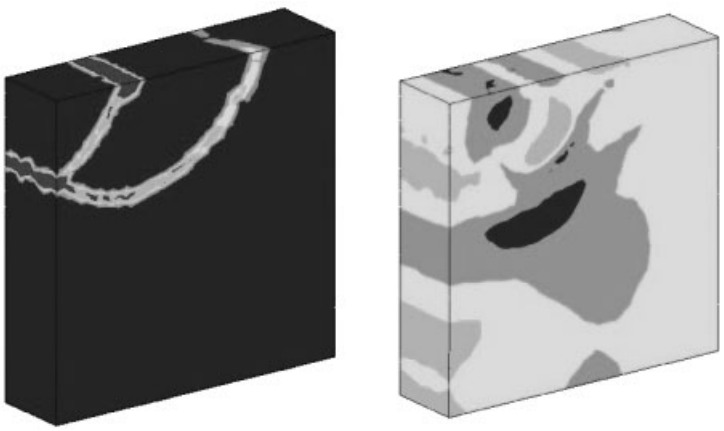

Figure 15. Equivalent plastic strain and pressure contour fills for 3D Prandtl's punch test with OSGS mixed formulations.

6. CONCLUSIONS

This paper presents the application of stabilized mixed linear simplicial elements (triangles and tetrahedra) to the solution of problems involving the capture of discontinuous solutions in J2 plasticity. Two stabilization methods, designed to allow equal-order interpolation of the displacement and pressure fields, are proposed: one based on the orthogonal sub-grid scales

(OSGS) approach and the GLS method, which can be considered a simplified version of the former. Both stabilization schemes are shown to attain control on the pressure field, completely removing global and local oscillations induced by the incompressibility constraints induced by J2 plastic flow. On one hand, the OSGS scheme is more appealing from the theoretical standpoint, as the corresponding stabilization terms decrease more rapidly upon mesh refinement. On the other hand, implementation of the GLS approach is somewhat simpler and requires less operations.

A consistent viscous regularization is also proposed and successfully applied, which allows to overcome the convergence difficulties often encountered in applications involving softening behaviour and strain localization. The derived method yields a robust scheme, suitable for engineering applications in 2D and 3D.

Numerical examples demonstrate the tremendous advantage of the mixed displacement/pressure formulation over the irreductible one to predict correct failure mechanisms with localized patterns of plastic deformation, which are practically free from any dependence of the mesh directional bias. Also, stabilization techniques are shown to alleviate the volumetric locking exhibited by non-stable formulations, yielding an improved global response in the softening regime.

ACKNOWLEDGEMENTS

The authors gratefully acknowledge the inestimable help of Prof. R. Codina, expressed in the form of unfailing suggestions and discussions.

REFERENCES

1. de Borst R. Some recent issues in computational failure mechanics. *International Journal for Numerical Methods in Engineering* 2001; **52**:63–95.
2. de Borst R. Fracture in quasi-brittle materials: a review of continuum damage-based approaches. *Engineering Fracture Mechanics* 2002; **69**:95–112.
3. Oliver J. A consistent characteristic length for smeared cracking models. *International Journal for Numerical Methods in Engineering* 1989; **28**:461–474.
4. Oliver J, Cervera M, Manzoli O. Strong discontinuities and continuum plasticity models: the strong discontinuity approach. *International Journal of Plasticity* 1999; **15**:1–34.
5. Wells GN, Sluys LJ, de Borst R. A *p*-adaptive scheme for overcoming volumetric locking during plastic flow. *Computer Methods in Applied Mechanics and Engineering* 2002; **191**:3153–3164.
6. Zienkiewicz OC, Taylor RL. *The Finite Element Method*. Butterworth-Heinemann: Oxford, 2000.
7. Zienkiewicz OC, Pastor M, Huang M. Softening, localization and adaptive remeshing: capture of discontinuous solutions. *Computational Mechanics* 1995; **17**:98–106.
8. Zienkiewicz OC, Huang M, Pastor M. Localization problems in plasticity using finite elements with adaptive remeshing. *International Journal for Numerical Methods in Geomechanics* 1995; **19**:127–148.
9. Pastor M, Li T, Liu X, Zienkiewcz OC. Stabilized linear triangles for failure problems in undrained soils. In *Proceedings of IV World Congress on Computational Mechanics*: '*Computational Mechanics: New Trends and Applications*', Idelshon S, Oñate E, Dvorkin E (eds). CIMNE: Barcelona, Spain, 1998.
10. Pastor M, Li T, Liu X, Zienkiewcz OC, Quecedo M. A fractional step algorithm allowing equal order interpolation for coupled analysis of saturated soil problems. *Mechanics of Cohesive-Frictional Materials* 2000; **5**:511–534.
11. Bonet J, Burton AJ. A simple average nodal pressure tetrahedral element for incompressible and nearly incompressible dynamic explicit applications. *Communications in Numerical Methods in Engineering* 1998; **14**: 437–449.
12. Zienkiewicz OC, Rojek J, Taylor RL, Pastor M. Triangles and tetrahedra in explicit dynamic codes for solids. *International Journal for Numerical Methods in Engineering* 1998; **43**:565–583.
13. Klaas O, Maniatty A, Shephard MS. A stabilized mixed finite element method for finite elasticity. Formulation for linear displacement and pressure interpolation. *Computer Methods in Applied Mechanics and Engineering* 1999; **180**:65–79.

14. Taylor RL. A mixed formulation for triangular and tetrahedral elements. In *Conference Proceedings on Métodos Numéricos en Ingeniería*, Abascal R, Domínguez J, Bugeda G (eds). SEMNI: Barcelona, Spain, 1999.
15. Dohrmann CR, Heinstein MW, Jung J, Key SW, Witkowsky WR. Node-based uniform strain elements for three-node triangular and four-node tetrahedral meshes. *International Journal for Numerical Methods in Engineering* 2000; **47**:1549–1568.
16. Taylor RL. A mixed-enhanced formulation for tetrahedral elements. *International Journal for Numerical Methods in Engineering* 2000; **47**:205–227.
17. Bonet J, Marriot H, Hassan O. An averaged nodal deformation gradient linear tetrahedral element for large strain explicit dynamic applications. *Communications in Numerical Methods in Engineering* 2001; **17**:551–561.
18. Bonet J, Marriot H, Hassan O. Stability and comparison of different linear tetrahedral formulations for nearly incompressible explicit dynamic applications. *International Journal for Numerical Methods in Engineering* 2001; **50**:119–133.
19. Oñate E, Rojek J, Taylor RL, Zienkiewicz OC. Linear triangles and tetrahedra for incompressible problem using a finite calculus formulation. *Proceedings of European Conference on Computational Mechanics, ECCM*: Cracow, Poland, 2001.
20. de Souza Neto EA, Pires FMA, Owen DRJ. A new F-bar-method for linear triangles and tetrahedra in the finite strain analysis of nearly incompressible solids. *Proceedings of VII International Conference on Computational Plasticity, COMPLAS*: Barcelona, Spain, 2003.
21. Hughes TJR. Multiscale phenomena: Green's function, Dirichlet-to Neumann formulation, subgrid scale models, bubbles and the origins of stabilized formulations. *Computer Methods in Applied Mechanics and Engineering* 1995; **127**:387–401.
22. Codina R, Blasco J. A finite element method for the Stokes problem allowing equal velocity-pressure interpolations. *Computer Methods in Applied Mechanics and Engineering* 1997; **143**:373–391.
23. Hughes TJR, Feijoó GR, Mazzei L, Quincy JB. The variational multiscale method—a paradigm for computational mechanics. *Computer Methods in Applied Mechanics and Engineering* 1998; **166**:3–28.
24. Codina R. Stabilization of incompressibility and convection through orthogonal sub-scales in finite element methods. *Computer Methods in Applied Mechanics and Engineering* 2000; **190**:1579–1599.
25. Chiumenti M, Valverde Q, Agelet de Saracibar C, Cervera M. A stabilized formulation for incompressible elasticity using linear displacement and pressure interpolations. *Computer Methods in Applied Mechanics and Engineering* 2002; **191**:5253–5264.
26. Chiumenti M, Valverde Q, Agelet de Saracibar C, Cervera M. A stabilized formulation for incompressible plasticity using linear triangles and tetrahedra. *International Journal of Plasticity* 2004; in press.
27. Cervera M, Chiumenti M, Valverde Q, Agelet de Saracibar C. Mixed linear/linear simplicial elements for incompressible elasticity and plasticity. *Computer Methods in Applied Mechanics and Engineering* 2003; **192**: 5249–5263.
28. Simo JC, Hughes TJR. *Computational inelasticity*. *Interdisciplinary Applied Mathematics*, vol. 7. Springer: Berlin, 1998.
29. Brezzi F, Fortin M. *Mixed and Hybrid Finite Element Methods*. Springer: New York, 1991.
30. Hughes TJR, Franca LP, Balestra M. A new finite element formulation for computational fluid dynamics: V. circumventing the Babuska–Brezzi condition: a stable Petrov–Galerkin formulation of the Stokes problem accomodating equal-order interpolations. *Computer Methods in Applied Mechanics and Engineering* 1986; **59**:85–99.
31. Hughes TJR, Franca LP, Hulbert GM. A new finite element formulation for computational fluid dynamics: VIII. The Galerkin/least-square method for advective–diffusive equations. *Computer Methods in Applied Mechanics and Engineering* 1989; **73**:173–189.
32. Cervera M, Agelet de Saracibar C, Chiumenti M. COMET: COupled MEchanical and Thermal analysis. Data Input Manual, Version 5.0, *Technical Report* IT-308, 2002, www.cimne.upc.es.
33. GiD: the personal pre and post processor, 2002, www.cimne.upc.es.

